

Parametric model for post-processing visibility ensemble forecasts

Ágnes Baran and Sándor Baran*

Faculty of Informatics, University of Debrecen, Hungary

Abstract

Despite the continuous development of the different operational ensemble prediction systems over the past decades, ensemble forecasts still might suffer from lack of calibration and/or display systematic bias, thus require some post-processing to improve their forecast skill. Here we focus on visibility, which quantity plays a crucial role e.g. in aviation and road safety or in ship navigation, and propose a parametric model where the predictive distribution is a mixture of a gamma and a truncated normal distribution, both right censored at the maximal reported visibility value. The new model is evaluated in two case studies based on visibility ensemble forecasts of the European Centre for Medium-Range Weather Forecasts covering two distinct domains in Central and Western Europe and two different time periods. The results of the case studies indicate that climatology is substantially superior to the raw ensemble; nevertheless, the forecast skill can be further improved by post-processing, at least for short lead times. Moreover, the proposed mixture model consistently outperforms the Bayesian model averaging approach used as reference post-processing technique.

Keywords: Bayesian model averaging, ensemble calibration, predictive distribution, visibility

1 Introduction

Despite the continuous development of autoland, autopilot, navigation and radar systems, visibility conditions are still critical in aviation and road safety and in ship navigation as well. In this way, reliable prediction of this weather quantity, defined by the World Meteorological Organization (WMO) as “the greatest distance at which a black object of suitable dimensions (located on the ground) can be seen and recognized when observed against the horizon sky” (WMO, 1992), results in a direct economic benefit.

Visibility forecasts are generated with the help of numerical weather prediction (NWP) models either as direct model outputs or by utilizing various algorithms (see e.g. Stoelinga

*Corresponding author: baran.sandor@inf.unideb.hu

and Warner, 1999; Gultepe *et al.*, 2006; Wagh *et al.*, 2023) to calculate visibility from forecasts of related weather quantities such as, for instance, precipitation or relative humidity (Chmielecki and Raftery, 2011). Nowadays, the state-of-the-art approach to weather prediction is to issue ensemble forecasts by running an NWP model several times with varying initial conditions or model parametrizations (Bauer *et al.*, 2015; Buizza, 2018a). In addition to providing a point forecast with a given forecast horizon for a given location and time point, a forecast ensemble allows assessing forecast uncertainty and even estimating the probability distribution of the future weather variable. Hence, the ensemble method opens the door for probabilistic forecasting (Gneiting and Raftery, 2005) and provides an important tool for forecast-based decision making (Fundel *et al.*, 2019). In particular, several recent studies (see Pahlavan *et al.*, 2021; Parde *et al.*, 2022) verify the superiority of probabilistic predictions e.g. in fog forecasting, which is one of the most frequent reasons of low visibility.

By now, all major weather centres operate ensemble prediction systems (EPSs); however, only a few has visibility among the forecasted parameters. For instance, since 2015, visibility is part of the Integrated Forecast System (IFS; ECMWF, 2021) of the European Centre for Medium-Range Weather Forecasts (ECMWF; ECMWF Directorate, 2012), and one can also mention the multimodel Short-Range Ensemble Forecast System of the National Centers for Environmental Prediction, which covers the Continental US, Alaska, and Hawaii regions (Zhou *et al.*, 2009).

Despite the tremendous development the EPSs have undergone in the last decades, ensemble forecasts are still often underdispersive and may also subject to systematic bias. This feature has been observed with several operational EPSs (see e.g. Buizza *et al.*, 2005) and can be corrected with some form of post-processing (Buizza, 2018b). In the last decades a large variety of statistical calibration techniques have been proposed for a broad range of weather parameters, for an overview of the most advanced approaches see Wilks (2018) or Vannitsem *et al.* (2021). Non-parametric methods usually represent predictive distributions via their quantiles estimated by some form of quantile regression (see e.g. Friederichs and Hense, 2007; Bremnes, 2019), whereas parametric models such as Bayesian model averaging (BMA; Raftery *et al.*, 2005) or ensemble model output statistics (EMOS; Gneiting *et al.*, 2005) provide full predictive distributions of the weather variables at hand. The BMA predictive probability density function (PDF) of a future weather quantity is the weighted sum of individual PDFs corresponding to the ensemble members. The weights are based on the relative performance of the members during a given training period, while an individual PDF can be considered as the conditional PDF of the future weather variable, provided the corresponding forecast is the best. This form of the predictive PDF might be beneficial in situations when multimodal predictive distributions are required (see e.g. Baran *et al.*, 2019), and the BMA models of various weather quantities differ only in the distribution families representing the mixture components. The essentially simpler EMOS model (also referred to as non-homogeneous regression) specifies the predictive distribution by a single parametric law with parameters connected to the ensemble members via appropriate link functions. Furthermore, recently machine learning-based approaches gain more and more popularity in ensemble post-processing both in parametric framework (see e.g. Rasp and Lerch, 2018; Ghazvinian *et al.*, 2021) and in non-parametric context (Bremnes, 2020); for a systematic

overview of the state-of-the-art techniques see Schultz and Lerch (2022). Finally, in the case of discrete quantities, such as total cloud cover (TCC), the predictive distribution is a probability mass function and post-processing can be considered as a classification problem, where both parametric techniques (Hemri *et al.*, 2016) and advanced machine learning-based classifiers can be applied (Baran *et al.*, 2021).

Although the predictive performance of visibility ensemble forecasts is highly below the skill of ensemble forecasts of other weather parameters such as temperature, wind speed or precipitation accumulation (see e.g. Zhou *et al.*, 2012), only a few of the above mentioned methods is adapted to this particular variable. Chmielecki and Raftery (2011) consider a BMA approach where each individual predictive PDF consists of a point mass at the maximal reported visibility and a beta distribution, which models the remaining visibility values. Ryerson and Hacker (2018) propose a non-parametric method for calibrating short-range visibility predictions obtained using the Weather Research and Forecasting Model (Ryerson and Hacker, 2014). Furthermore, since most synoptic observation (SYNOP) stations report visibility in discrete values according to the WMO suggestions, in a recent study Baran and Lakatos (2023) investigate the approach of Hemri *et al.* (2016) and Baran *et al.* (2021), and obtain (discrete) predictive distributions of visibility with the help of proportional odds logistic regression and multilayer perceptron neural network classifiers.

In the present article, we develop a novel parametric post-processing model for visibility ensemble forecasts where the predictive distribution is a mixture of a gamma and a truncated normal distribution, both right censored at the maximal reported visibility value. The proposed mixture model is applied in two case studies that focus on ECMWF visibility ensemble forecasts covering two distinct domains in Central and Western Europe and two different time periods. As reference post-processing approach we consider the BMA model of Chmielecki and Raftery (2011); nonetheless, we report the predictive performance of climatological and raw ensemble forecasts as well.

The paper is organized as follows. Section 2 briefly introduces the visibility datasets considered in the case studies. The proposed mixture model, the reference BMA approach, training data selection procedures and tools of forecast verification are provided in Section 3, followed by the results for the two case studies presented in Section 4. Finally, concluding remarks and lessons learned can be found in Section 5.

2 Data

In the case studies of Section 4 we evaluate the mixture model proposed in Section 3.1 using ECMWF visibility ensemble forecasts (given in 1 m steps) and corresponding validating observations (reported in 10 m increments) covering two different time periods and having disjoint but geographically close ensemble domains. In fact, we consider subsets of the datasets studied in Baran and Lakatos (2023) by selecting only those locations where the resolution of the reported observations is close to that of the forecasts and can be considered as continuous.

The first dataset comprises the operational 51-member ECMWF visibility ensemble fore-

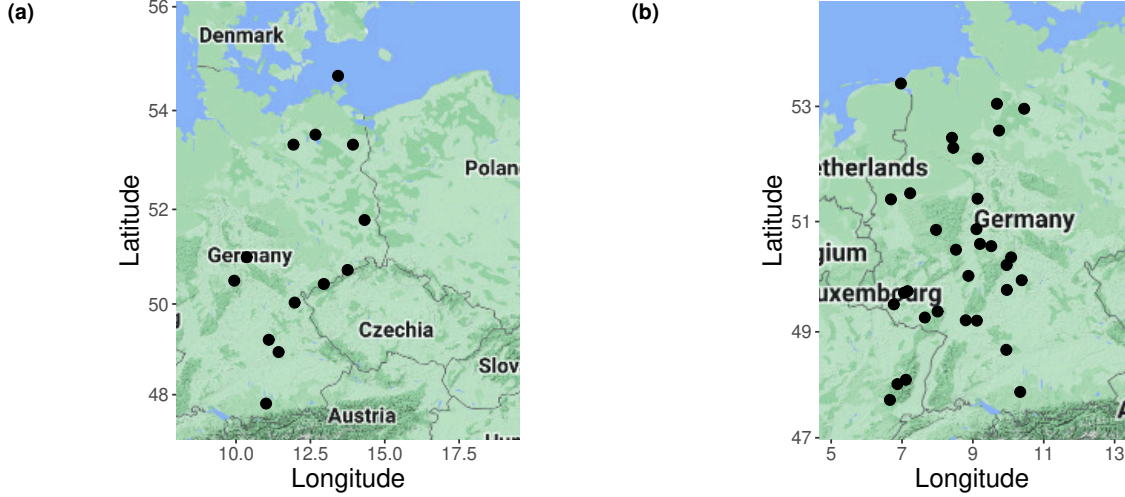


Figure 1: Locations of SYNOP observation stations corresponding to (a) ECMWF forecasts for 2020-2021; (b) EUPPBench benchmark dataset.

casts (control forecast (CTRL) and 50 members (ENS) generated using random perturbations) for calendar years 2020 and 2021 initialized at 0000 UTC with a forecast horizon of 240 h and a temporal resolution of 6 h (a total of 40 forecasts) for 13 SYNOP stations in the eastern part of Germany (Figure 1a). In terms of observations this dataset is complete and there are just two days with incomplete predictions; namely, there are no exchangeable ensemble members in 132 h ahead forecasts initialized 2 June 2021 and 114 h ahead forecasts initialized 17 December 2021.

We also consider visibility data of the *EUPPBench* benchmark dataset (Demaeyer *et al.*, 2023) for calendar years 2017 – 2018 for 32 SYNOP stations in Germany and France (Figure 1b). Here the 51-member operational ECMWF ensemble is extended with the high-resolution (HRES) prediction. All forecasts are initialized at 0000 UTC and 20 different lead times from 6 h to 120 h with a time step of 6 h are studied. In contrast to the other dataset, in the *EUPPBench* benchmark data there are no missing forecasts; however, around 2% of the forecast cases lacks station observations.

3 Parametric post-processing of visibility

As mentioned in the Introduction, EMOS is a simple and efficient tool for post-processing ensemble weather forecasts (see also Vannitsem *et al.*, 2021). However, as it fits a single probability law to the forecast ensemble chosen from a given parametric distribution family, EMOS is usually not flexible enough to model multimodal predictive distributions. A natural approach is to consider a mixture of several probability laws, which is also the fundamental idea of the BMA models. Furthermore, visibility is non-negative and the reported observations are often limited to a certain value (in our case studies to 75 and 70 km), which restriction should be taken into account, too. A possible solution is to censor a non-negative predictive distribution from above or to mix a continuous law and a point mass at the max-

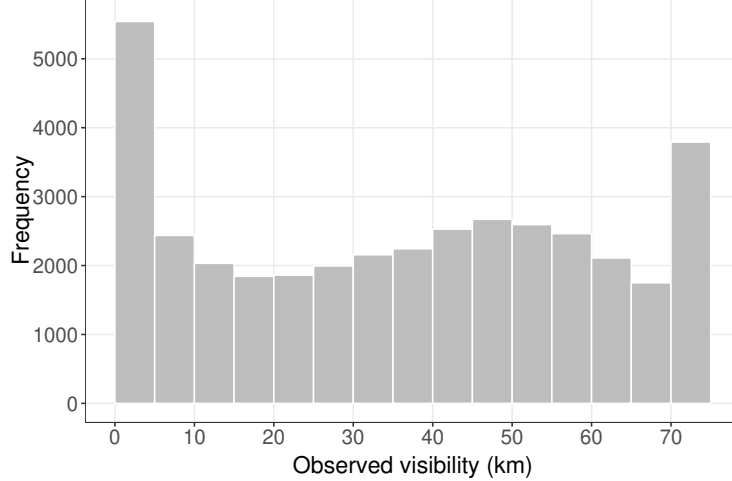


Figure 2: Climatological frequency histogram of visibility for calendar years 2020 – 2021.

imal reported visibility value. The former approach appears in the mixture model proposed in Section 3.1, whereas the reference BMA model of Chmielecki and Raftery (2011) described briefly in Section 3.2 is an example of the latter.

In the following sections, let f_1, f_2, \dots, f_{52} denote a 52-member ECMWF visibility ensemble forecasts for a given location, time point and forecast horizon, where $f_1 = f_{HRES}$ and $f_2 = f_{CTRL}$ are the high-resolution and control members, respectively, whereas f_3, f_4, \dots, f_{52} correspond to the 50 members generated using perturbed initial conditions. These members, which we will denote by $f_{ENS,1}, f_{ENS,2}, \dots, f_{ENS,50}$, lack individually distinguishable physical features, hence they are statistically indistinguishable and can be treated as exchangeable. In what follows, \bar{f}_{ENS} and S_{ENS} will denote the mean and standard deviation of the 50 exchangeable ensemble members, respectively, and following the suggestions of e.g. Fraley *et al.* (2010) or Wilks (2018), in the models presented in Sections 3.1 and 3.2 these members will share the same parameters.

3.1 Mixture model

According to the climatological histogram of Figure 2, a unimodal distribution is clearly not appropriate to model visibility. One has to handle separately low visibility values, there is a second hump at medium to large visibility and a censoring is required at the maximal reported value x_{\max} .

Let $g(x|\kappa, \theta)$ and $G(x|\kappa, \theta)$ denote the probability density function (PDF) and cumulative distribution function (CDF) of a gamma distribution $\Gamma(\kappa, \theta)$ with shape $\kappa > 0$ and scale $\theta > 0$, respectively, while notations $h(x|\mu, \sigma^2)$ and $H(x|\mu, \sigma^2)$ are used for the PDF and the CDF of a normal distribution $\mathcal{N}_0(\mu, \sigma^2)$ with location μ , scale $\sigma > 0$ left truncated at zero. Furthermore, denote by $g^c(x|\kappa, \theta)$ and $h^c(x|\mu, \sigma^2)$ the PDFs of the

censored versions of these laws, that is

$$\begin{aligned} g^c(x|\kappa, \theta) &:= g(x|\kappa, \theta)\mathbb{I}_{\{x < x_{\max}\}} + (1 - G(x_{\max}|\kappa, \theta))\mathbb{I}_{\{x = x_{\max}\}}, \\ h^c(x|\mu, \sigma^2) &:= h(x|\mu, \sigma^2)\mathbb{I}_{\{x < x_{\max}\}} + (1 - H(x_{\max}|\mu, \sigma^2))\mathbb{I}_{\{x = x_{\max}\}}, \end{aligned}$$

where \mathbb{I}_A denotes the indicator function of a set A .

The proposed predictive distribution of visibility is a mixture of censored gamma and censored truncated normal distributions

$$p(x|\kappa, \theta, \mu, \sigma^2, \omega) = (1 - \omega)g^c(x|\kappa, \theta) + \omega h^c(x|\mu, \sigma^2), \quad (3.1)$$

where both the weight $\omega \in [0, 1]$ and the parameters of the component distributions depend on the ensemble forecast. In particular,

$$\omega = 1 / (1 + \exp(-\gamma \bar{f}_{ENS})),$$

which is a smooth monotone function of \bar{f}_{ENS} . Furthermore, the mean $m = \kappa\theta$ and variance $v = \kappa\theta^2$ of the uncensored gamma distribution $\Gamma(\kappa, \theta)$ are given as

$$m = a_0 + a_1^2 f_{HRES} + a_2^2 f_{CTRL} + a_3^2 \bar{f}_{ENS} + a_4 B_1(d) + a_5 B_2(d) \quad \text{and} \quad v = b_0 + b_1^2 S_{ENS}^2,$$

while location and scale of the truncated normal distribution $\mathcal{N}_0(\mu, \sigma^2)$ are expressed as

$$\mu = \alpha_0 + \alpha_1^2 f_{HRES} + \alpha_2^2 f_{CTRL} + \alpha_3^2 \bar{f}_{ENS} + \alpha_4 B_1(d) + \alpha_5 B_2(d) \quad \text{and} \quad \sigma = \beta_0 + \beta_1^2 S_{ENS},$$

where functions $B_1(d)$ and $B_2(d)$ are annual base functions

$$B_1(d) := \sin(2\pi d/365) \quad \text{and} \quad B_2(d) := \cos(2\pi d/365) \quad (3.2)$$

addressing seasonal variations in the mean/location (see e.g. Dabering *et al.*, 2017) and d denotes the day of the year. Following the optimum score principle of Gneiting and Raftery (2007), model parameters $\gamma, a_0, a_1, \dots, a_5, \alpha_0, \alpha_1, \dots, \alpha_5, b_0, b_1, \beta_0, \beta_1 \in \mathbb{R}$ are estimated by optimizing the mean value of an appropriate proper scoring rule, namely the logarithmic score (see Section 3.4), over an appropriate training data set comprising past forecast-observation pairs. In the case when the high-resolution and/or the control forecast is not available, one obviously sets $a_1 = \alpha_1 = 0$ and/or $a_2 = \alpha_2 = 0$.

3.2 Bayesian model averaging

The BMA predictive distribution of visibility X based on 52-member ECMWF ensemble forecasts is given by

$$\mathbf{p}(x|f_1, f_2, \dots, f_{52}, \boldsymbol{\theta}_1, \boldsymbol{\theta}_2, \dots, \boldsymbol{\theta}_{52}) = \sum_{k=1}^{52} \omega_k \mathbf{h}(x|f_k; \boldsymbol{\theta}_k), \quad (3.3)$$

where ω_k is the weight and $\mathbf{h}(x|f_k; \boldsymbol{\theta}_k)$ is the component PDF corresponding to the k th ensemble member with parameter vector $\boldsymbol{\theta}_k$ to be estimated with the help of the training

data. Note that weights form a probability distribution ($\omega_k \geq 0$, $k = 1, 2, \dots, 52$, and $\sum_{k=1}^{52} \omega_k = 1$) and ω_k represents the relative performance of the forecast f_k in the training data.

In the BMA model of Chmielecki and Raftery (2011) the conditional PDF $\mathfrak{h}(x|f_k; \boldsymbol{\theta}_k)$ is based on the square root of the forecast f_k and consists of two parts. The first models the point mass at the maximal reported visibility x_{\max} using logistic regression as

$$\text{logit } \mathbf{P}(X = x_{\max}|f_k) = \log \frac{\mathbf{P}(X = x_{\max}|f_k)}{\mathbf{P}(X < x_{\max}|f_k)} = \pi_{0k} + \pi_{1k}f_k^{1/2}. \quad (3.4)$$

The second part provides a continuous model of visibility given that it is less than x_{\max} using a beta distribution with shape parameters $\alpha, \beta > 0$ and support $[0, x_{\max}]$ defined by PDF

$$q(x|\alpha, \beta) := \frac{(y/x_{\max})^{\alpha-1} (1 - y/x_{\max})^{\beta-1}}{\mathcal{B}(\alpha, \beta)x_{\max}}, \quad x \in [0, x_{\max}],$$

where $\mathcal{B}(\alpha, \beta)$ is the beta function. Given the k th ensemble member f_k , the mean $x_{\max} \alpha/(\alpha + \beta)$ and standard deviation $x_{\max} \sqrt{\alpha\beta/((\alpha + \beta)\sqrt{\alpha + \beta + 1})}$ of the corresponding beta distribution are expressed as

$$\mathbf{m}_k = \varrho_{0k} + \varrho_{1k}f_k^{1/2} \quad \text{and} \quad \mathbf{s}_k = c_0 + c_1f_k^{1/2}, \quad (3.5)$$

respectively. Note that variance parameters in (3.5) are kept constant for practical reasons. On the one hand, this form reduces the number of unknown parameters to be estimated and helps in avoiding overfitting. On the other hand, as argued by Sloughter *et al.* (2007) and Chmielecki and Raftery (2011), in a more general model allowing member-dependent variance parameters c_{0k} and c_{1k} , these parameters do not vary much from one forecast to another.

Now, the conditional PDF of visibility given the k th ensemble member f_k is

$$\mathfrak{h}(x|f_k; \boldsymbol{\theta}_k) = \mathbf{P}(X < x_{\max}|f_k) \mathbf{q}(x|f_k) \mathbb{I}_{\{X < x_{\max}\}} + \mathbf{P}(X = x_{\max}|f_k) \mathbb{I}_{\{X = x_{\max}\}}$$

where $\mathbf{P}(X = x_{\max}|f_k)$ is defined by (3.4), $\mathbf{q}(x|f_k)$ denotes the beta distribution with mean and standard deviation specified by (3.5) and $\boldsymbol{\theta}_k := (\pi_{0k}, \pi_{1k}, \varrho_{0k}, \varrho_{1k}, c_0, c_1)$.

Parameters π_{0k} and π_{1k} are estimated from the training data by logistic regression, mean parameters ϱ_{0k} and ϱ_{1k} are obtained using linear regression connecting the visibility observations less than x_{\max} to the square roots of the corresponding ensemble members, whereas for estimating weights ω_k and variance parameters c_0, c_1 one uses the maximum likelihood approach with EM algorithm to maximize the likelihood function. For more details we refer to Chmielecki and Raftery (2011) and note that following again Fraley *et al.* (2010), we do not distinguish between the exchangeable ensemble members f_3, f_4, \dots, f_{52} and assume $\omega_3 = \omega_4 = \dots = \omega_{52}$ and $\boldsymbol{\theta}_3 = \boldsymbol{\theta}_4 = \dots = \boldsymbol{\theta}_{52}$. Furthermore, if some of the ensemble forecasts are missing, then the corresponding weights should be set to zero.

3.3 Training data selection

As discussed, parameters of both the novel mixture model introduced in Section 3.1 and the BMA approach presented in Section 3.2 are estimated with the help of training data consisting past forecast-observation pairs. In the case studies of Section 4 each lead time is treated separately and we consider rolling training windows, which is a standard approach in parametric post-processing. This means that training data for a given day d and lead time ℓ comprises forecasts of the given horizon and corresponding observations for the n -day time interval between calendar days $d - \ell - n + 1$ and $d - \ell$. The optimal length of the rolling training period is usually determined by comparing the predictive performance of post-processed forecasts corresponding to different values of n .

Besides the temporal range of the training data, its spatial composition is also a key point in forecast calibration. The simplest and most parsimonious approach is the regional modelling (Thorarinsdottir and Gneiting, 2010), which is based on training data of the whole ensemble domain and all investigated locations share a single set of parameters. Regional models require quite short training periods and allow an extrapolation of the predictive distribution to locations where only forecasts are available (see e.g. Baran and Baran, 2022); however, as argued e.g. by Lerch and Baran (2017) or Baran *et al.* (2020), they are not suitable for large and heterogeneous domains. In contrast, local models result in distinct parameter estimates for different locations as they are based only on the training data of each particular site. Local models usually outperform their regional counterparts, provided the training period is long enough for reliable parameter estimation. For instance, Hemri *et al.* (2014) suggest 720-, 365- and 1816-day rolling training periods for EMOS modelling of temperature, wind speed and precipitation accumulation, respectively. Finally, the advantages of regional and local parameter estimation can be combined by the use of semi-local techniques, where either training data of a given location is augmented with data of sites with similar characteristics, or the ensemble domain is divided into more homogeneous subdomains and, within each subdomain, a regional modelling is performed. In the case studies of Section 4, besides local and regional parameter estimation, we also consider the clustering-based semi-local approach suggested by Lerch and Baran (2017). For a given date of the verification period, to each observation station we first assign a feature vector depending both on the station climatology and the forecast errors of the raw ensemble mean over the training period. Then, based on the corresponding feature vectors, the stations are grouped into homogeneous clusters using k -means clustering and dynamically regrouped as the training period rolls ahead.

3.4 Model verification

As argued by Gneiting and Raftery (2007), the evaluation of forecast skill should be based on the “paradigm of maximizing the sharpness of the predictive distributions subject to calibration.” The former refers to the concentration of the probabilistic forecasts, while the latter means a statistical consistency between the predictive distributions and the corresponding validating observations. Calibration and sharpness can be addressed simultaneously with

the help of proper scoring rules, which are loss functions quantifying predictive performance by assigning numerical values to forecast-observation pairs. In atmospheric sciences probably the most popular scoring rules are the logarithmic score (LogS; Good, 1952), that is the negative logarithm of the predictive PDF evaluated at the validating observation, and the continuous ranked probability score (CRPS; Wilks, 2019, Section 9.5.1). For a forecast provided in the form of a CDF F and a real value x representing the verifying observation, the CRPS is defined as

$$\text{CRPS}(F, x) := \int_{-\infty}^{\infty} [F(y) - \mathbb{I}_{\{y \geq x\}}]^2 dy = \mathbb{E}|X - x| - \frac{1}{2}\mathbb{E}|X - X'|, \quad (3.6)$$

where \mathbb{I}_H denotes the indicator function of a set H , while X and X' are independent random variables distributed according to F with finite first moment. Both the LogS and the CRPS are negatively oriented scores, that is smaller values mean better predictive performance. In most applications the CRPS has a simple closed form (see e.g. Jordan *et al.*, 2019); however, this is not the case for the predictive distributions corresponding to the mixture and BMA models of Sections 3.1 and 3.2, respectively. In such cases, based on the representation on the right hand side of (3.6), which also implies that the CRPS can be reported in the same units as the observation, one can consider the Monte Carlo approximation of the CRPS based on a large sample drawn from F (see e.g. Krüger *et al.*, 2021). In the case studies of Section 4, the predictive performance of the various forecasts with a given lead time are compared using the mean CRPS over all forecast cases in the validation period.

Furthermore, the forecast skill of the competing forecasts with respect to dichotomous events can be quantified with the help of the mean Brier score (BS; Wilks, 2019, Section 9.4.2). For a predictive CDF F and the event that the observed visibility x does not exceed a given threshold y , the BS is defined as

$$\text{BS}(F, x; y) := [F(y) - \mathbb{I}_{\{y \geq x\}}]^2,$$

so the CRPS is just the integral of the BS over all possible thresholds.

For a probabilistic forecast F , one can assess the improvement with respect to a reference forecast F_{ref} in terms of a score \mathcal{S} by using the corresponding skill score (Murphy, 1973), defined as

$$\mathcal{SS}_F := 1 - \frac{\overline{\mathcal{S}}_F}{\overline{\mathcal{S}}_{F_{\text{ref}}}},$$

where $\overline{\mathcal{S}}_F$ and $\overline{\mathcal{S}}_{F_{\text{ref}}}$ denote the mean score values corresponding to forecasts F and F_{ref} , respectively. Skill scores are positively oriented (the larger the better), and in our case studies we report the continuous ranked probability skill score (CRPSS) and the Brier skill score (BSS).

Calibration and sharpness can also be investigated by examining the coverage and average width of $(1-\alpha)100\%$, $\alpha \in]0, 1[$, central prediction intervals (intervals between the lower and upper $\alpha/2$ quantiles of the predictive distribution). Coverage is defined as the proportion of validating observations located in this interval and for a properly calibrated predictive distribution this value should be around $(1-\alpha)100\%$. Note that level α is usually chosen

to match the nominal coverage of $(K - 1)/(K + 1)100\%$ of a K -member ensemble, which allows a direct comparison with the raw forecasts.

Further simple tools for assessing calibration of probabilistic forecasts are the verification rank histogram (or Talagrand diagram) of ensemble predictions and the probability integral transform (PIT) histogram of forecasts given in the form of predictive distributions. The Talagrand diagram is the histogram of ranks of the verifying observations with respect to the corresponding ensemble forecasts (see e.g. Wilks, 2019, Section 9.7.1), and in the case of a properly calibrated K -member ensemble the verification ranks should be uniformly distributed on $\{1, 2, \dots, K + 1\}$. The PIT is the value of the predictive CDF evaluated at the verifying observation with a possible randomization in the points of discontinuity (see e.g. Wilks, 2019, Section 9.5.4). The PIT values of calibrated predictive distributions follow a standard uniform law and in this way the PIT histogram can be considered as the continuous counterpart of the verification rank histogram.

Furthermore, the accuracy of point forecasts such as mean and median can be quantified with the help of the root mean squared error (RMSE) and mean absolute error (MAE), where the former is optimal for the mean, whereas the latter is for the median forecast (Gneiting, 2011).

Finally, to get insight into the uncertainty in verification scores and significance of score differences, some of the the skill scores are accompanied with 95% confidence intervals. These intervals are based on 2000 block bootstrap samples obtained using the stationary bootstrap scheme with mean block length derived according to Politis and Romano (1994).

4 Results

The predictive performance of the novel mixture model introduced in Section 3.1 is tested on the two datasets of ECMWF visibility ensemble forecasts and corresponding observations described in Section 2. As reference we consider the BMA approach provided in Section 3.2, climatological forecasts (observations of a given training period are considered as a forecast ensemble) and the raw ECMWF ensemble as well. Both parametric post-processing models require rather large training data to ensure reliable parameter estimation; moreover, seasonal variations of visibility should also be taken into account during the modelling process. In the case of the mixture model this latter requirement is addressed with the use of the annual base functions (3.2) in the locations of the component distributions. Hence, one can consider long training periods, which besides regional modelling allows clustering-based semi-local or even local parameter estimation, too. In the following sections regional, clustering-based semi-local and local mixture models are referred to as *Mixed-R*, *Mixed-C* and *Mixed-L*, respectively. In contrast to the mixture model, there is no seasonality included in the BMA predictive distribution, so short training periods are preferred allowing only regional modelling. BMA models of both Sections 4.1 and 4.2 are based on 25-day rolling training periods, which length is a result of a detailed data analysis (comparison of various BMA verification scores for a whole calendar year for training periods of 20, 25, 30, 35 and 40 days). Note that this training period length is identical to the one suggested by Chmielecki

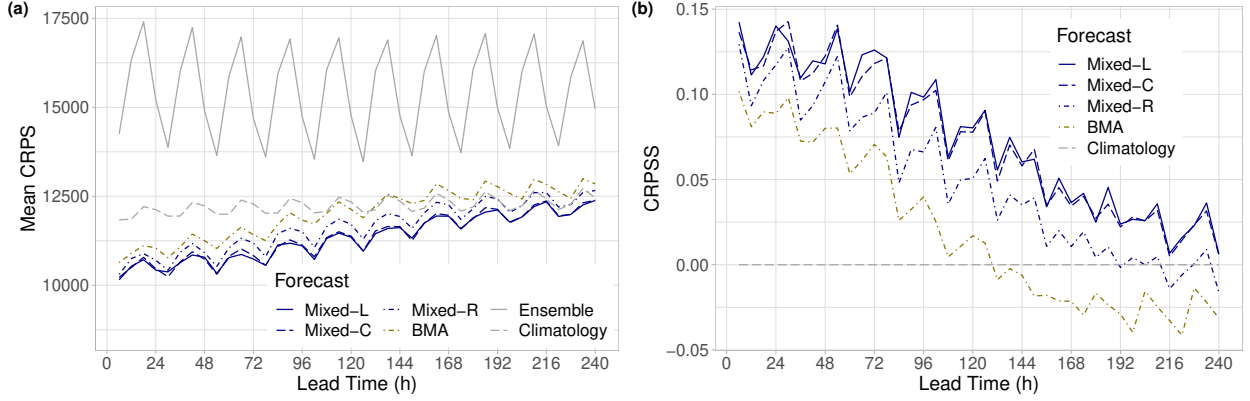


Figure 3: Mean CRPS of post-processed, raw and climatological visibility forecasts for calendar year 2021 (a) and CRPSS of post-processed forecasts with respect to climatology (b) as functions of the lead time.

Mixed-L	Mixed-C	Mixed-R	BMA	Climatology
73.44 %	73.60 %	75.41 %	77.85 %	79.34 %

Table 1: Overall mean CRPS of post-processed and climatological visibility forecasts for calendar year 2021 as proportion of the mean CRPS of the raw ECMWF ensemble.

and Raftery (2011). Furthermore, as mentioned, for both calibration approaches separate modelling is performed for each lead time. Finally, in both case studies the size of the climatological forecasts matches the size of the corresponding raw ensemble predictions, that is in Section 4.1 observations of 51-day rolling training periods (see Section 3.3) are considered, whereas in Section 4.2 climatology is based on 52 past observations.

4.1 Calibration of 51-member visibility ensemble forecasts

In this case study the predictive performance of the competing forecasts is compared using data of calendar year 2021. For the 51-member ECMWF ensemble (control forecast and 50 exchangeable members) the mixture model has 15 free parameters to be estimated, and the comparison of the forecast skill of regional models based on training periods of length 100, 150, \dots , 350 days reveals that the longest considered training period results in the best predictive performance. This 350-day training window is kept also for local and semi-local modelling, where the 13 locations are grouped into 6 clusters. Semi-local models with 3, 4 and 5 clusters have also been tested; however, these models slightly underperform the chosen one. Furthermore, as mentioned, the 11 parameters of the BMA model are estimated regionally using 25-day rolling training periods, which means a total of 325 forecast cases for each training step. Hence, the data/parameter ratio of the regional BMA approach ($325/11=29.5$) is slightly above of the corresponding ratio of the local mixture model ($350/15=23.3$). Note that in this case study validating visibility observations are reported up to 75 km, hence the

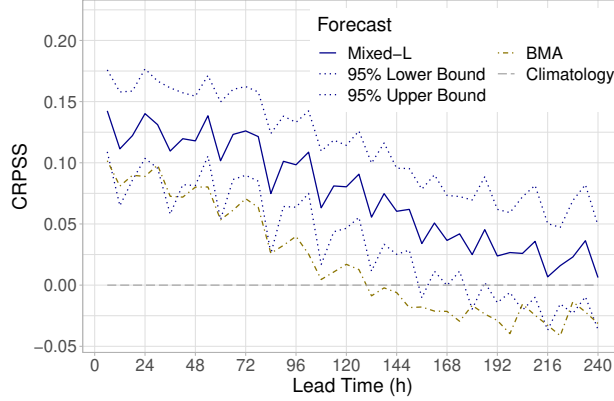


Figure 4: CRPSS with respect to climatology of the best performing mixed model (together with 95 % confidence intervals) and the BMA approach for calendar year 2021 as functions of the lead time.

support of all investigated post-processing models is limited to the 0 – 75 km interval with a point mass at the upper bound.

Figure 3a indicates that in terms of the mean CRPS all investigated forecasts outperform the raw visibility ensemble by a wide margin. The diurnal oscillation in the CRPS is a result of the different observation times (0000, 0600, 1200 and 1800 UTC), and the raw ensemble exhibits the strongest dependence on the time of the day having the highest skill at 0600 UTC. Parametric models are superior to climatology only for shorter forecast horizons and their advantage gradually fades with the increase of the lead time. The difference between post-processed forecasts and climatology is more visible in the CRPSS values of Figure 3b. Skill scores of the locally and semi-locally trained mixture models are positive for all lead times and the difference between these forecasts is negligible. Up to 192 h the Mixed-R approach also outperforms climatology and it is clearly ahead of the BMA, which results in positive CRPSS only for shorter forecast horizons (6 – 126 h). This ranking of the competing methods is also confirmed by Table 1 providing the overall mean CRPS values of calibrated and climatological forecasts as proportions of the mean CRPS of the raw ECMWF visibility ensemble. Note that the good performance of climatology is fully in line with the results of Chmielecki and Raftery (2011).

In Figure 4 the CRPSS values of the best performing locally trained mixture model are accompanied with 95 % confidence intervals, which provides some insight into the significance of the differences in CRPS. The superiority of the Mixed-L forecast over climatology in terms of the mean CRPS is significant at a 5 % level up to 150 h and between 42 h and 174 h significantly outperforms the BMA model as well. We remark that for the latter approach after 96 h the CRPSS with respect to climatology fails to be significantly positive (not shown).

The analysis of Brier skill scores plotted in Figure 5 slightly tones the picture about the performance of post-processed forecasts. For visibility not exceeding 1 km, none of the competitors outperforms climatology (Figure 5a) and calibrated predictions are superior to

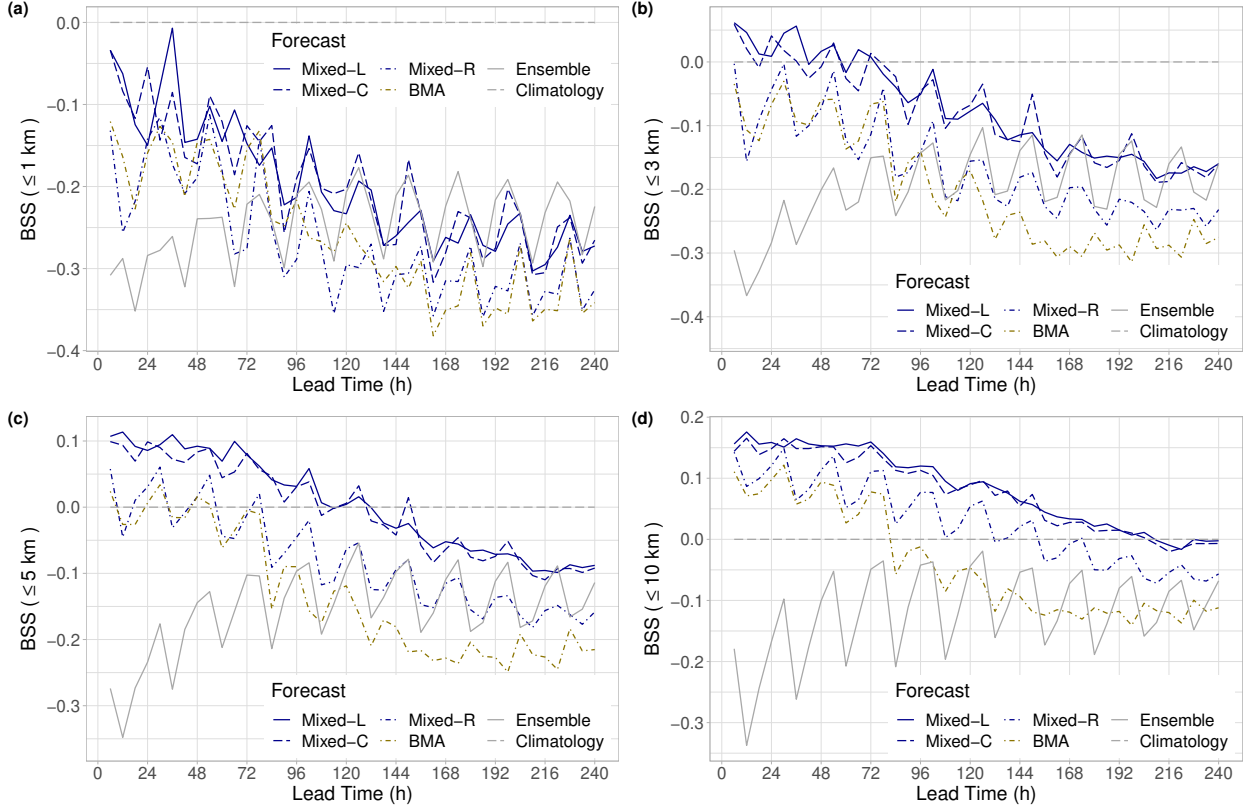


Figure 5: BSS of raw and post-processed visibility forecasts for calendar year 2021 with respect to climatology for thresholds 1 km (a), 3 km (b), 5 km (c) and 10 km (d) as functions of the lead time.

raw ensemble forecasts only for short lead times. With the increase of the threshold the positive effect of post-processing is getting more and more pronounced and the ranking of the different models starts matching the one based on the mean CRPS. From the competing calibration methods the locally and semi-locally trained mixed models consistently display the highest skill and for the largest threshold value of 10 km they outperform climatology up to 204 h (Figure 5d).

The verification rank and PIT histograms of Figure 6 again illustrate the primacy of climatology over the raw ensemble and the improved calibration of post-processed forecasts. Raw ECMWF visibility forecasts are underdispersive and tend to overestimate the observed visibility; however, these deficiencies improve with the increase of the forecast horizon. Climatology results in almost uniform rank histograms with just a minor underdispersion and there is no visible dependence on the forecast horizon. Unfortunately, none of the four investigated post-processing models can completely eliminate the bias of the raw visibility forecasts, which is slightly more pronounced for longer lead times.

Furthermore, the coverage values of nominal 96.15 % central prediction intervals depicted in Figure 7a are fairly consistent with the shapes of the corresponding verification rank and PIT histograms. The underdispersion of the raw ensemble is confirmed with its low coverage, which shows an increasing trend, a clear diurnal cycle, and ranges from 25.58 % to

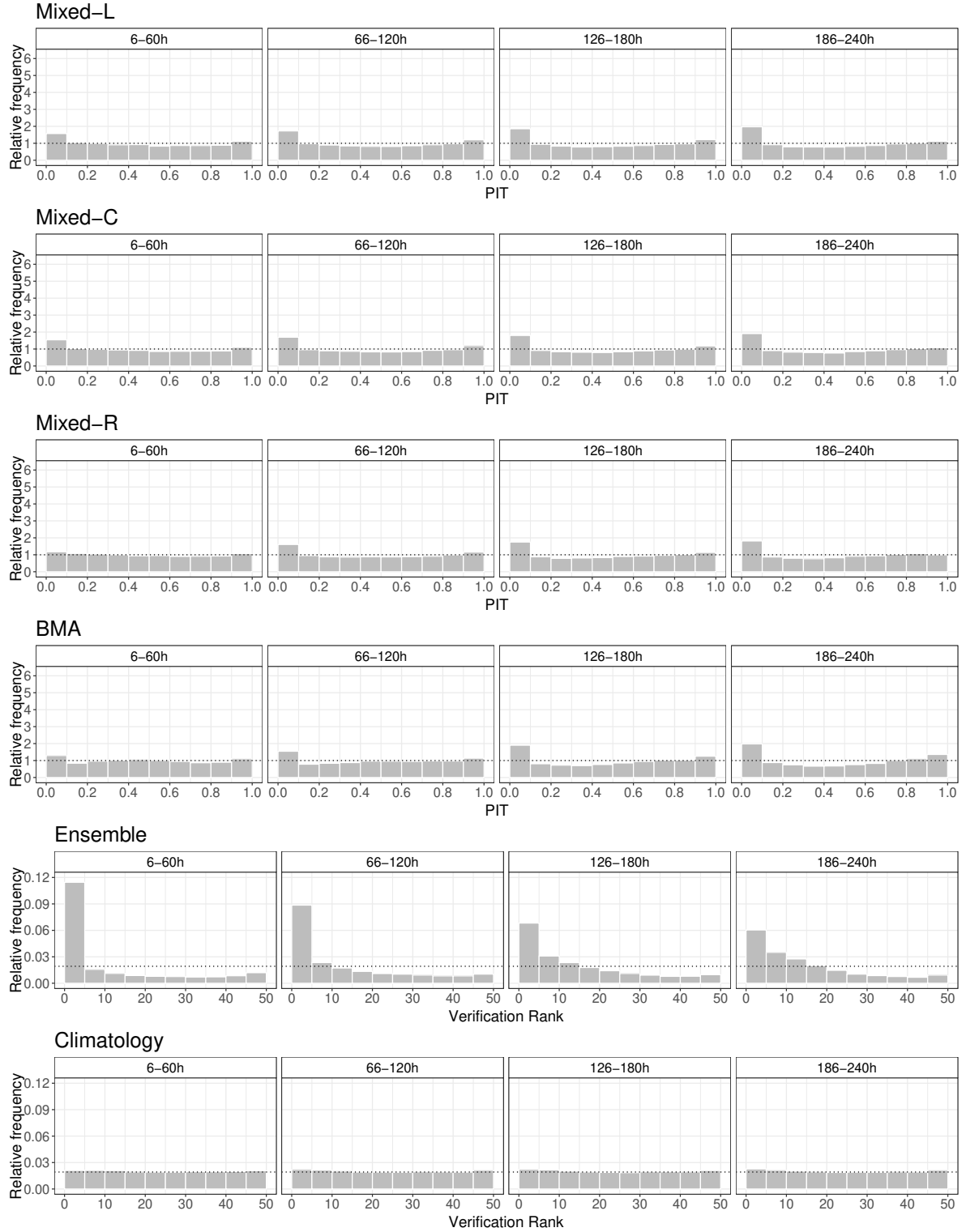


Figure 6: PIT histograms of post-processed and verification rank histograms of climatological and raw visibility forecasts for calendar year 2021 for lead times 6–60 h, 66–120 h, 126–180 h and 186–240 h.

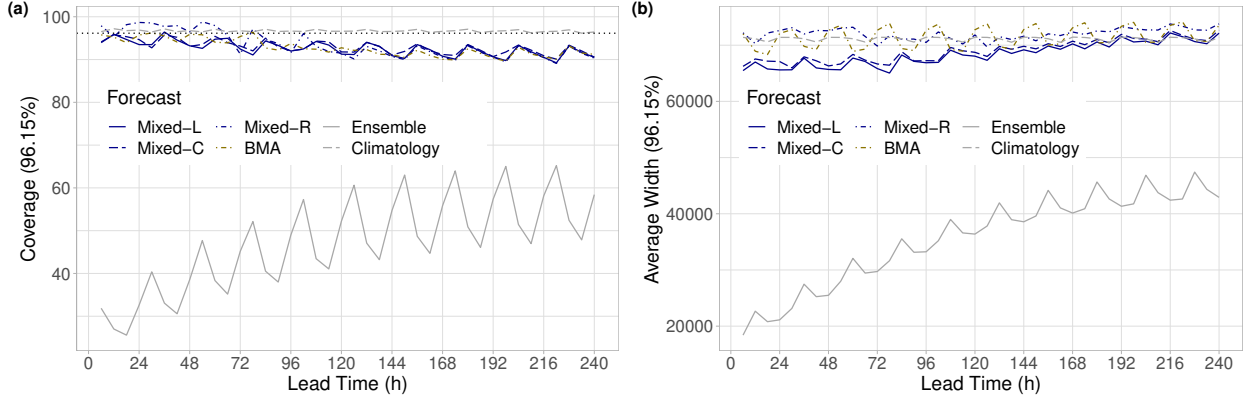


Figure 7: Coverage (a) and average width (b) of nominal 96.15 % central prediction intervals of raw and post-processed visibility forecasts for calendar year 2021 as functions of the lead time. In panel (a) the ideal coverage is indicated by the horizontal dotted line.

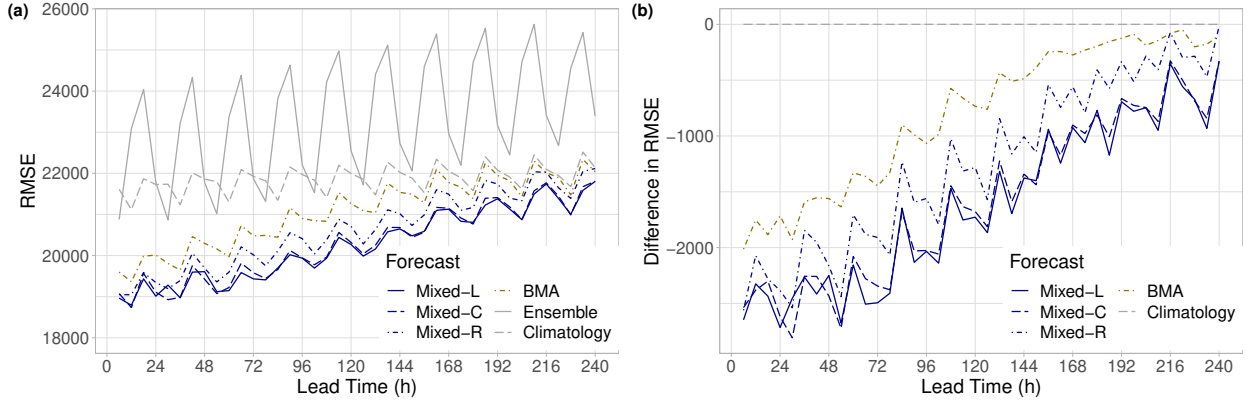


Figure 8: RMSE of the mean forecasts for calendar year 2021 (a) and difference in RMSE from climatology (b) as functions of the lead time.

65.21 %. As one can observe on the corresponding curve of Figure 7b, the improvement of the ensemble coverage with the increase of the forecast horizon is a consequence of the increase in spread, that results in expanding central prediction intervals. The price of the almost perfect coverage of climatology with a mean absolute deviation from the nominal value of 0.53 % is the much wider central prediction interval. The coverage values of post-processed forecasts decrease with the increase of the lead time, the corresponding mean absolute deviations from the nominal 96.15 % are 3.55 % (Mixed-L), 3.21 % (Mixed-C), 3.55 % (Mixed-R) and 3.39 % (BMA). However, this negative trend in coverage, especially in the case of the locally and semi-locally trained mixed models, is combined with increasing average width, which can be a consequence of the growing bias.

Finally, in terms of the RMSE of the mean forecast, all post-processing approaches outperform both the raw ensemble and climatology for all lead times (see Figure 8a); however, their advantage over climatology is negatively correlated with the forecast horizon. Mixed-L

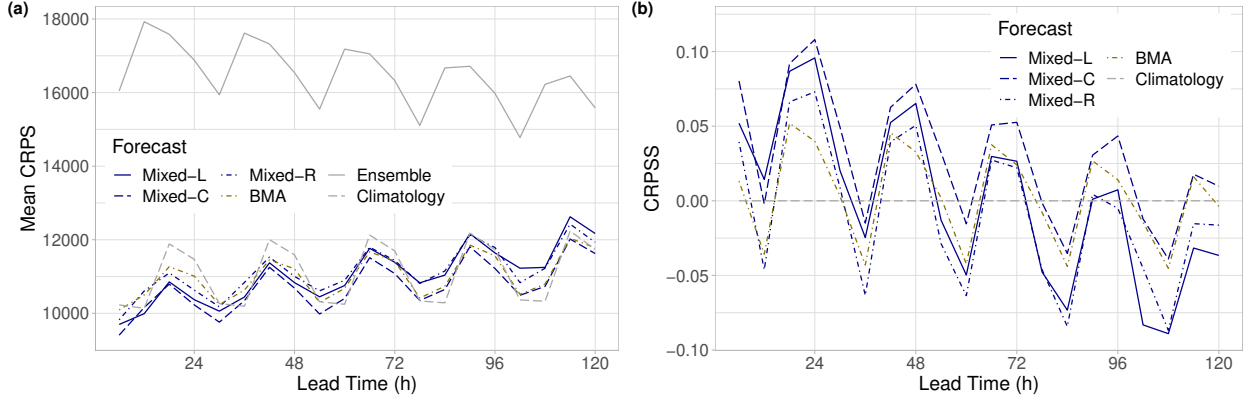


Figure 9: Mean CRPS of post-processed, raw and climatological EUPPBench visibility forecasts for calendar year 2018 (a) and CRPSS of post-processed forecasts with respect to climatology (b) as functions of the lead time.

Mixed-L	Mixed-C	Mixed-R	BMA	Climatology
66.90 %	64.96 %	67.41 %	66.80 %	67.28 %

Table 2: Overall mean CRPS of post-processed and climatological EUPPBench visibility forecasts for calendar year 2018 as proportion of the mean CRPS of the raw ECMWF ensemble.

and Mixed-C approaches result in the lowest RMSE values, followed by the Mixed-R and BMA forecasts (see also Figure 8b), which order perfectly matches the ranking based on the mean CRPS (Figure 3b) and the mean BS for all studied thresholds (Figure 5).

4.2 Calibration of EUPPBench visibility ensemble forecasts

Since in the EUPPBench benchmark dataset the 51-member ECMWF ensemble forecast is augmented with the deterministic high-resolution prediction, the mixture model (3.1) has 17 free parameters to be estimated, whereas for the BMA predictive PDF (3.3), the parameter vector is 16 dimensional. As mentioned, BMA modelling is based on 25-day regional training, while in order to determine the optimal training period length for mixed models, we again compare the skill of the regionally estimated forecasts based on rolling training windows of 100, 150, \dots , 350 days. In the case of the EUPPBench visibility data the skill of the different models is compared with the help of forecast-observation pairs for calendar year 2018. In contrast to the previous case study, where the longest tested training period of 350 days is preferred, here the 100-day window results in the best overall performance. Using the same training period length we again investigate local modelling and semi-local estimation based on 4 clusters. Taking into account the maximal reported visibility observation in the EUPPBench benchmark dataset, now the mixed and BMA predictive distributions have point masses at 70 km.

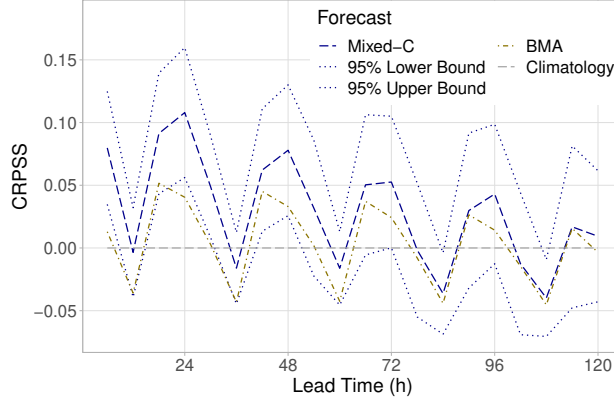


Figure 10: CRPSS with respect to climatology of the best performing mixed model (together with 95 % confidence intervals) and the BMA approach for calendar year 2018 as functions of the lead time.

Again, Figure 9a shows the mean CRPS of post-processed, raw and climatological EUPP-Bench visibility forecasts as functions of the lead time, while in Figure 9b the CRPSS values of the mixed and BMA models with respect to the 52-day climatology are plotted. Similar to the case study of Section 4.1, climatological and post-processed forecasts outperform the raw ensemble by a wide margin; however, now the advantage of post-processing over climatology is not so obvious and the ranking of the calibration methods also differ. From the four investigated models the Mixed-C model results in the lowest mean CRPS for all lead times but 12 h; nevertheless, even this approach shows negative skill against climatology for lead times corresponding to 1200 UTC observations. Local modelling (Mixed-L) is competitive only for short forecast horizons, which might be explained by the short training period leading to numerical issues during parameter estimation due to the low data/parameter ratio. In general, the skill scores of all post-processing methods show a decreasing trend with the BMA having the mildest slope. Based on Table 2, providing the improvement in the overall mean CRPS over the raw ECMWF ensemble, one can establish ranking Mixed-C – BMA – Mixed-L – Climatology – Mixed-R. Note that the improvements provided here are much larger than the ones in Table 1 and in terms of the mean CRPS the 52-member EUPPBench visibility forecasts are behind the more recent 51-member ensemble predictions studied in Section 4.1. This dissimilarity in forecast performance is most likely due to the consecutive improvement in the ECMWF IFS; however, it might also be related to the difference in the forecast domains (see Figure 1).

Furthermore, according to Figure 10, even for 0000, 0600 and 1800 UTC observations the advantage of the best performing Mixed-C model over climatology is significant at a 5 % level only up to 48 h, whereas the difference in skill from the BMA approach is significant just at 6 h, 24 h and 30 h. Note that the CRPSS of the BMA model with respect to climatology is significantly positive at a 5 % only for lead times 18 h, 24 h, 40 h and 48 h (not shown).

The Brier skill scores of Figure 11 lead us to similar consequences as in the previous case study. For the lowest threshold of 1 km, all forecasts underperform climatology (Figure 11a);

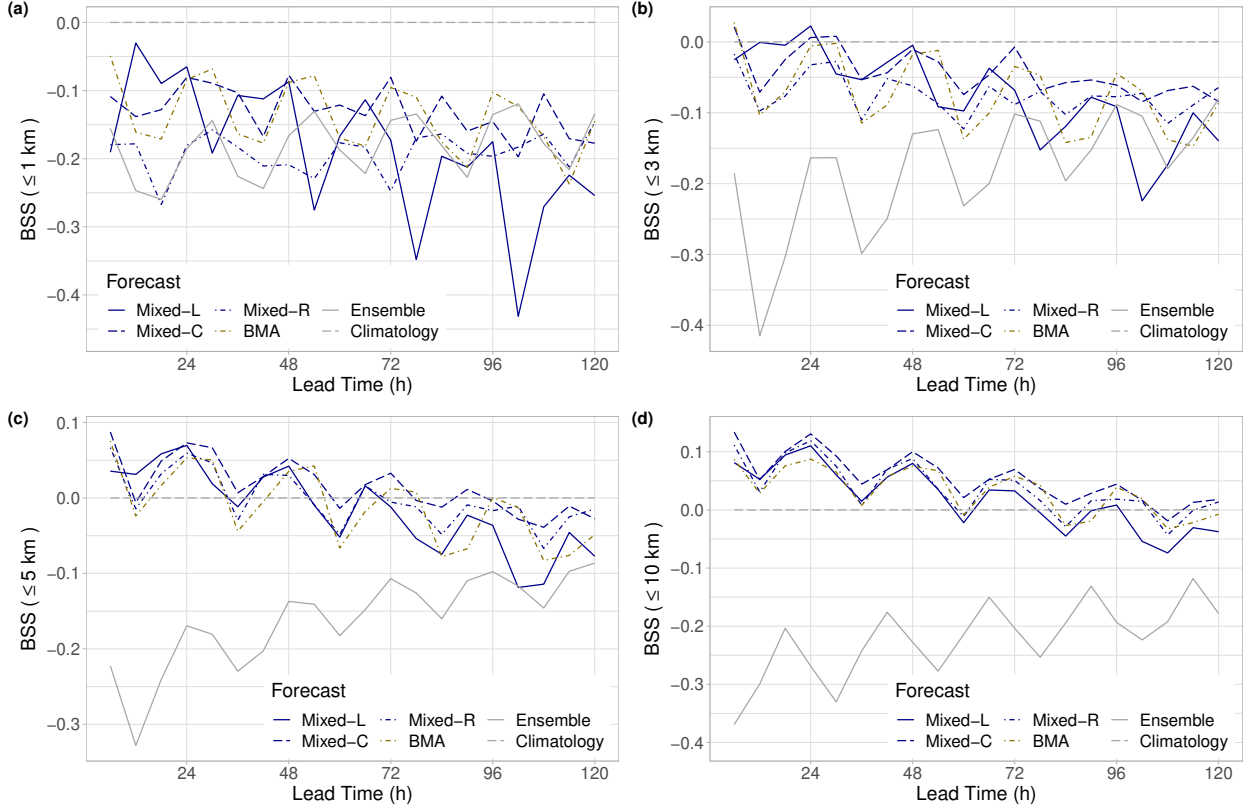


Figure 11: BSS of raw and post-processed EUPPBench visibility forecasts for calendar year 2018 with respect to climatology for thresholds 1 km (a), 3 km (b), 5 km (c) and 10 km (d) as functions of the lead time.

however, the skill of post-processed predictions improves when the threshold is increased. For 3, 5 and 10 km threshold the ranking of the various models is again identical to the ordering based on the mean CRPS (see Figure 9b) with the Mixed-C approach exhibiting the best overall predictive performance, closely followed by the BMA model. For the largest threshold of 10 km, up to 54 h, climatology is outperformed even by the least skillful Mixed-L approach (see Figure 11d), whereas the leading semi-locally trained mixed model results in a positive BSS up to 102 h.

The verification rank histograms of the raw EUPPBench visibility forecasts depicted in Figure 12 show a much stronger bias than the corresponding panel of Figure 6, while the improvement with the increase of the forecast horizon is less pronounced. Climatology is also slightly biased but in the opposite direction, whereas the verification rank histograms of all post-processed forecasts are closer to the desired uniform distribution than in the case study of Section 4.1. Here the locally trained mixed model exhibits the strongest bias; however, neither the verification rank histograms of climatology, nor the PIT histograms of the calibrated forecasts indicate visible dependence on the forecast horizon.

The fair calibration of climatological and post-processed forecasts can also be observed in Figure 13a displaying the coverage values of the nominal 96.13 % central prediction intervals. Semi-locally and regionally trained mixed models and climatology result in almost perfect

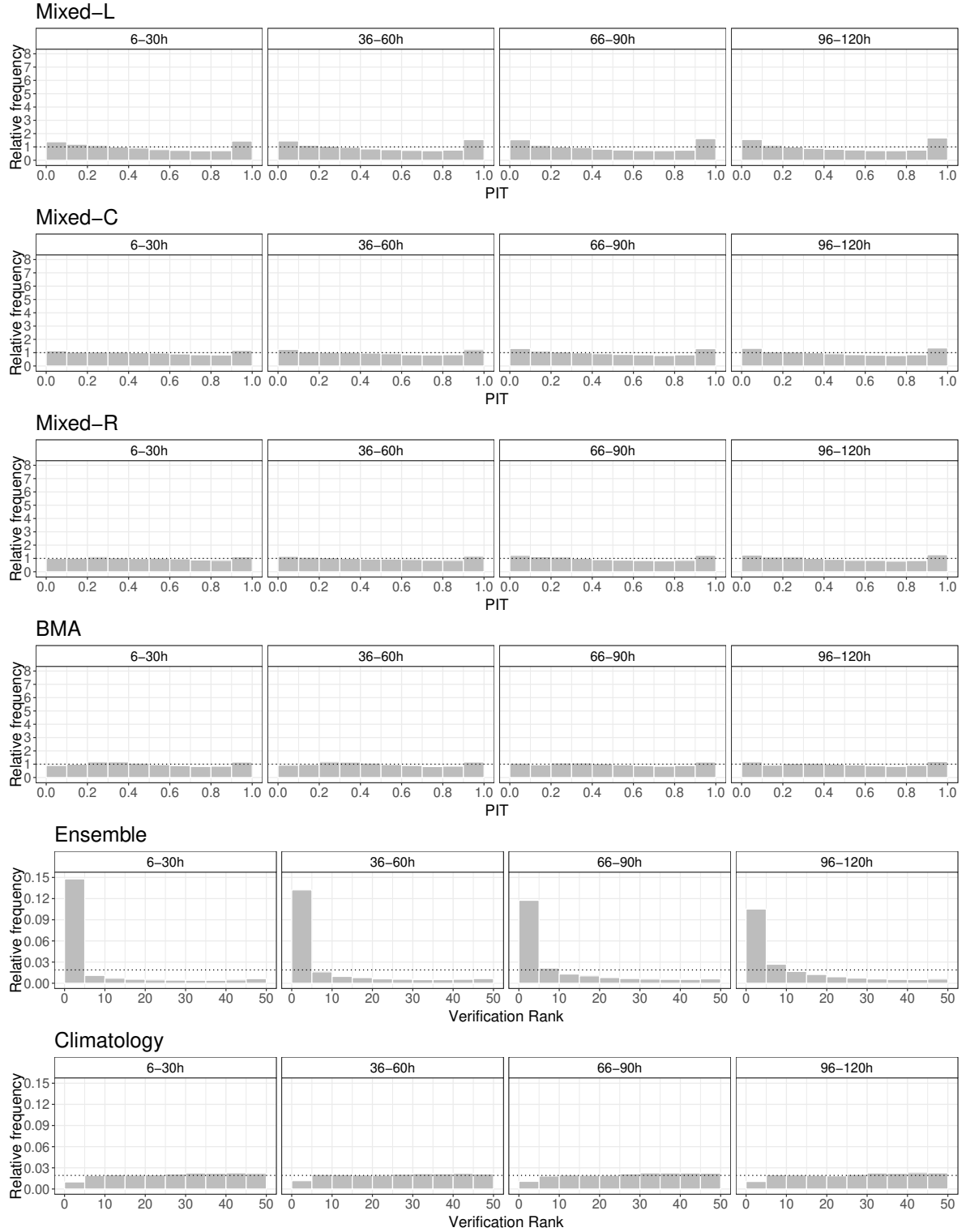


Figure 12: PIT histograms of post-processed and verification rank histograms of climatological and raw EUPPBench visibility forecasts for calendar year 2018 for lead times 6–30 h, 36–60 h, 66–90 h and 96–120 h.

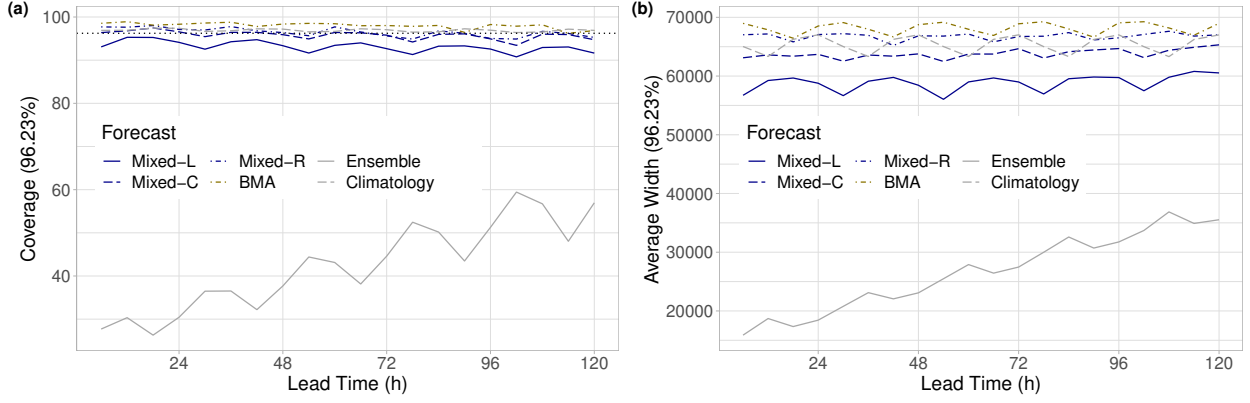


Figure 13: Coverage (a) and average widths (b) of nominal 96.23% central prediction intervals of raw and post-processed EUPPBench visibility forecasts for calendar year 2018 as functions of the lead time. In panel (a) the ideal coverage is indicated by the horizontal dotted line.

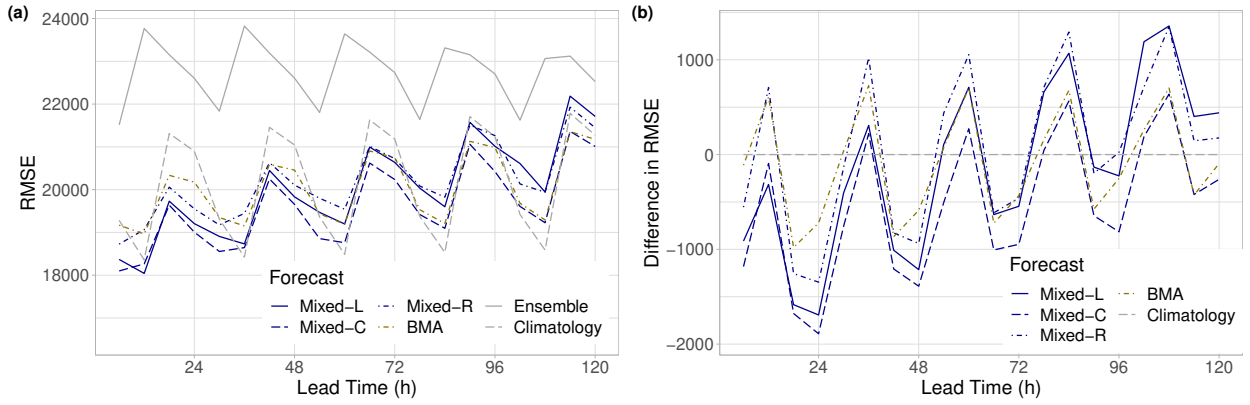


Figure 14: RMSE of the mean EUPPBench forecasts for calendar year 2018 (a) and difference in RMSE from climatology (b) as functions of the lead time.

coverage, closely followed by the BMA model; the corresponding mean absolute deviations from the nominal value are 0.69 %, 0.90 %, 0.72 % and 1.81 %, respectively. The Mixed-L model is slightly behind its competitors with a mean absolute deviation of 3.00 %, whereas the maximal coverage of the raw EUPPBench ensemble does not reach 60 %. Note that the ranking of the various predictions, the increasing coverage of the raw ensemble, and the lack of visible trend in the coverage values of post-processed forecasts and climatology is pretty much in line with the shapes of the corresponding histograms of Figure 12. In general, the average widths of the investigated 96.13 % central prediction intervals (Figure 13b) are rather consistent with the matching coverage values. Nevertheless, one should remark that the best performing Mixed-C model results in sharper predictions than climatology and the Mixed-R and BMA approaches.

Finally, according to Figure 14, in terms of the RMSE of the mean, we see a similar

behaviour and ranking of the different forecasts as in the case of the mean CRPS (see Figure 9). While the raw ensemble is clearly behind the other forecasts, with the increase of the lead time climatology becomes more and more competitive, especially at forecast horizons corresponding to 1200 UTC observations. However, up to 30 h, both locally and semi-locally trained mixed models result in lower RMSE than the climatological forecast, and the Mixed-C approach consistently outperforms all other calibration methods for all lead times but 12 h.

5 Conclusions

We propose a novel parametric approach to calibrating visibility ensemble forecasts, where the predictive distribution is a mixture of a gamma and a truncated normal law, both right censored at the maximal reported visibility. Three model variants that differ in the spatial selection of training data are evaluated in two case studies, where as reference post-processing method we consider the BMA model of Chmielecki and Raftery (2011); however, we also investigate the skill of climatological and raw ensemble forecasts. While both case studies are based on ECMWF visibility predictions with a 6 h temporal resolution, they cover distinct geographical regions and time intervals, and only one of them uses the deterministic high resolution forecast. The results presented in Section 4 indicate, that all post-processing models consistently outperform the raw ensemble by a wide margin and the real question is whether statistical calibration results in improvement compared to climatology. In the case of the 51-member operational ECMWF ensemble, e.g. in terms of the mean CRPS of the probabilistic and RMSE of the mean forecasts, the best performing locally and semi-locally trained mixed models outperform climatological predictions for all investigated lead times. For the EUPPBench dataset the situation is far from being so obvious; post-processing can result consistently positive skill with respect to climatology only up to 30 h. In general, the advantage of post-processed forecasts over climatology shows a decreasing trend with the increase of the forecast horizon, locally and semi-locally trained mixed models are preferred against the regionally estimated one, and the BMA approach is slightly behind the competitors. Note that the general conclusions about the effect of post-processing and the behaviour and ranking of the raw, climatological and calibrated visibility forecasts are almost completely in line with the results of Baran and Lakatos (2023), where classification-based discrete post-processing of visibility is studied based on extended versions of the current visibility datasets (more observation stations from the same geographical regions).

The results of this study suggest several further directions of future research. One possible option is to consider a matching distributional regression network (DRN) model, where the link functions connecting the parameters of the mixture predictive distribution with the ensemble forecast are replaced by an appropriate neural network. This parametric machine learning-based approach is proved successful for several weather quantities, such as temperature (Rasp and Lerch, 2018), precipitation (Ghazvinian *et al.*, 2021), wind gust (Schultz and Lerch, 2022), wind speed (Baran and Baran, 2021) or solar irradiance (Baran and Baran, 2022).

Furthermore, one can also investigate the impact of introduction of additional covariates on the forecast skill of parametric models based on the proposed censored gamma – truncated and censored normal mixture predictive distribution. In the DRN setup this step is rather straightforward and might result in significant improvement in predictive performance (see e.g Rasp and Lerch, 2018; Schultz and Lerch, 2022). A natural choice can be any further visibility forecast (for instance, the one of the Copernicus Atmospheric Monitoring Service); however, forecasts of other weather quantities affecting visibility can also be considered.

Finally, using two-step multivariate post-processing techniques one can extend the proposed mixture model in order to obtain spatially and/or temporally consistent calibrated visibility forecasts. For an an overview of the state-of-the-art multivariate approaches we refer to Lerch *et al.* (2020) and Lakatos *et al.* (2023).

Acknowledgments. The work leading to this paper was done in part during the visit of Sándor Baran to the Heidelberg Institute for Theoretical Studies in July 2023 as guest researcher. Both authors gratefully acknowledge the support of the the National Research, Development and Innovation Office under Grant No. K142849. Finally, the authors are indebted to Zied Ben Bouallègue for providing the ECMWF visibility data for 2020–2021.

References

- Baran, Á and Baran, S. (2022) A two-step machine learning approach to statistical post-processing of weather forecasts for power generation. *arXiv*: 2207.07589.
- Baran, Á., Lerch, S., El Ayari, M. and Baran, S. (2021) Machine learning for total cloud cover prediction. *Neural. Comput. Appl.* **33**, 2605–2620.
- Baran, S. and Baran, Á. (2021) Calibration of wind speed ensemble forecasts for power generation. *Időjárás* **125**, 609–624.
- Baran, S., Baran, Á., Pappenberger, F. and Ben Bouallègue, Z. (2020) Statistical post-processing of heat index ensemble forecasts: is there a royal road? *Q. J. R. Meteorol. Soc.* **146**, 3416–3434.
- Baran, S., Hemri, S. and El Ayari, M. (2019) Statistical post-processing of water level forecasts using Bayesian model averaging with doubly-truncated normal components. *Water Resour. Res.* **55**, 3997–4013.
- Baran, S. and Lakatos, M. (2023) Statistical post-processing of visibility ensemble forecasts. *Meteorol. Appl.*, doi:10.1002/met.2157.
- Bauer, P., Thorpe, A. and Brunet, G. (2015) The quiet revolution of numerical weather prediction. *Nature* **525**, 47–55.
- Bremnes, J. B. (2019) Constrained quantile regression splines for ensemble postprocessing. *Mon. Weather Rev.* **147**, 1769–1780.

- Bremnes, J. B. (2020) Ensemble postprocessing using quantile function regression based on neural networks and Bernstein polynomials. *Mon. Weather Rev.* **148**, 403–414.
- Buizza, R. (2018a) Introduction to the special issue on “25 years of ensemble forecasting”. *Q. J. R. Meteorol. Soc.* **145**, 1–11.
- Buizza, R. (2018b) Ensemble forecasting and the need for calibration. In Vannitsem, S., Wilks, D. S., Messner, J. W. (eds.), *Statistical Postprocessing of Ensemble Forecasts*. Elsevier, Amsterdam, pp. 15–48.
- Buizza, R., Houtekamer, P. L., Toth, Z., Pellerin, G., Wei, M. and Zhu, Y. (2005) A comparison of the ECMWF, MSC, and NCEP global ensemble prediction systems. *Mon. Weather Rev.* **133**, 1076–1097.
- Chmielecki, R. M. and Raftery, A. E. (2011) Probabilistic visibility forecasting using Bayesian model averaging. *Mon. Weather Rev.* **139**, 1626–1636.
- Dabernig, M., Mayr, G. J., Messner, J. W. and Zeileis, A. (2017) Spatial ensemble postprocessing with standardized anomalies. *Q. J. R. Meteorol. Soc.* **143**, 909–916.
- Demaeyer, J., Bhend, J., Lerch, S., Primo, C., Van Schaeybroeck, B., Atencia, A., Ben Bouallègue, Z., Chen, J., Dabernig, M., Evans, G., Faganelli Pucer, J., Hooper, B., Horat, N., Jobst, D., Merše, J., Mlakar, P., Möller, A., Mestre, O., Taillardat, M. and Vannitsem, S. (2023) The EUPPBench postprocessing benchmark dataset v1.0. *Earth Syst. Sci. Data* **15**, 2635–2653.
- ECMWF Directorate (2012) Describing ECMWF’s forecasts and forecasting system. *ECMWF Newsletter* **133**, 11–13.
- ECMWF (2021) *IFS Documentation CY47R3 - Part IV Physical processes*. ECMWF, Reading. Available at: <http://dx.doi.org/10.21957/eyrpir4vj> [Accessed on 25 October 2023]
- Fraley, C., Raftery, A. E. and Gneiting, T. (2010) Calibrating multimodel forecast ensembles with exchangeable and missing members using Bayesian model averaging. *Mon. Weather Rev.* **138**, 190–202.
- Friederichs, P. and Hense, A. (2007) Statistical downscaling of extreme precipitation events using censored quantile regression. *Mon. Weather Rev.* **135**, 2365–2378.
- Fundel, V. J., Fleischhut, N., Herzog, S. M., Göber, M. and Hagedorn, R. (2019) Promoting the use of probabilistic weather forecasts through a dialogue between scientists, developers and end-users. *Q. J. R. Meteorol. Soc.* **145**, 210–231.
- Ghazvinian, M., Zhang, Y., Seo, D.-J., He, M. and Fernando, N. (2021) A novel hybrid artificial neural network - parametric scheme for postprocessing medium-range precipitation forecasts. *Adv. Water Resour.* **151**, paper 103907.

- Gneiting, T. (2011) Making and evaluating point forecasts. *J. Amer. Statist. Assoc.* **106**, 746–762.
- Gneiting, T. and Raftery, A. E. (2005) Weather forecasting with ensemble methods. *Science* **310**, 248–249.
- Gneiting, T. and Raftery, A. E. (2007) Strictly proper scoring rules, prediction and estimation. *J. Amer. Statist. Assoc.* **102**, 359–378.
- Gneiting, T., Raftery, A. E., Westveld, A. H. and Goldman, T. (2005) Calibrated probabilistic forecasting using ensemble model output statistics and minimum CRPS estimation. *Mon. Weather Rev.* **133**, 1098–1118.
- Good, I. J. (1952) Rational decisions. *J. R. Stat. Soc. Series B Stat. Methodol.* **14**, 107–114.
- Gultepe, I., Müller, M. D. and Boybeyi, Z. (2006) A new visibility parameterization for warm-fog applications in numerical weather prediction models. *J. Appl. Meteorol. Climatol.* **45**, 1469–1480.
- Hemri, S., Haiden, T. and Pappenberger, F. (2016) Discrete postprocessing of total cloud cover ensemble forecasts. *Mon. Weather Rev.* **144**, 2565–2577.
- Hemri, S., Scheuerer, M., Pappenberger, F., Bogner, K. and Haiden, T. (2014) Trends in the predictive performance of raw ensemble weather forecasts. *Geophys. Res. Lett.* **41**, 9197–9205.
- Jordan, A., Krüger, F. and Lerch, S. (2019) Evaluating probabilistic forecasts with scoringRules. *J. Stat. Softw.* **90**, 1–37.
- Krüger, F., Lerch, S., Thorarinsdottir, T. L. and Gneiting, T. (2021). Predictive inference based on Markov chain Monte Carlo output. *Int. Stat. Rev.* **89**, 215–433.
- Lakatos, M., Lerch, S., Hemri, S. and Baran, S. (2023) Comparison of multivariate post-processing methods using global ECMWF ensemble forecasts. *Q. J. R. Meteorol. Soc.* **149**, 856–877.
- Lerch, S. and Baran, S. (2017) Similarity-based semi-local estimation of EMOS models. *J. R. Stat. Soc. Ser. C Appl. Stat.* **66**, 29–51.
- Lerch, S., Baran, S., Möller, A., Groß, J., Schefzik, R., Hemri, S. and Graeter, M. (2020) Simulation-based comparison of multivariate ensemble post-processing methods. *Nonlinear Process. Geophys.* **27**, 349–371.
- Murphy, A. H. (1973) Hedging and skill scores for probability forecasts. *J. Appl. Meteorol.* **12**, 215–223.
- Pahlavan, R., Moradi, M., Tajbakhsh, S., Azadi, M., Rahnama, M. (2021) Fog probabilistic forecasting using an ensemble prediction system at six airports in Iran for 10 fog events. *Meteorol. Appl.* **28**, paper e2033.

- Parde, A. N., Ghude, S. D., Dhangar, N. G., Lonkar, P., Wagh, S., Govardhan, G., Biswas, M., Jenamani, R. K. (2022) Operational probabilistic fog prediction based on ensemble forecast system: A decision support system for fog. *Atmosphere* **13**, paper 1608.
- Politis, D. N. and Romano, J. P. (1994) The stationary bootstrap. *J. Amer. Statist. Assoc.* **89**, 1303–1313.
- Raftery, A. E., Gneiting, T., Balabdaoui, F. and Polakowski, M. (2005) Using Bayesian model averaging to calibrate forecast ensembles. *Mon. Weather Rev.* **133**, 1155–1174.
- Rasp, S. and Lerch, S. (2018) Neural networks for postprocessing ensemble weather forecasts. *Mon. Weather Rev.* **146**, 3885–3900.
- Ryerson, W. R. and Hacker, J. P. (2014) The potential for mesoscale visibility predictions with a multimodel ensemble. *Wea. Forecasting* **29**, 543–562.
- Ryerson, W. R. and Hacker, J. P. (2018) A nonparametric ensemble postprocessing approach for short-range visibility predictions in data-sparse areas. *Wea. Forecasting* **33**, 835–855.
- Schultz, B. and Lerch, S. (2022) Machine learning methods for postprocessing ensemble forecasts of wind gusts: a systematic comparison. *Mon. Weather Rev.* **150**, 235–257.
- Sloughter, J. M., Raftery, A. E., Gneiting, T. and Fraley, C. (2007) Probabilistic quantitative precipitation forecasting using Bayesian model averaging. *Mon. Weather Rev.* **135**, 3209–3220.
- Stoelinga, T. G. and Warner, T. T. (1999) Nonhydrostatic, mesobeta-scale model simulations of cloud ceiling and visibility for an east coast winter precipitation event. *J. Appl. Meteorol. Climatol.* **38**, 385–404.
- Thorarinsdottir, T. L. and Gneiting, T. (2010) Probabilistic forecasts of wind speed: ensemble model output statistics by using heteroscedastic censored regression. *J. R. Stat. Soc. Ser. A Stat. Soc.* **173**, 371–388.
- Vannitsem, S., Bremnes, J. B., Demaeyer, J., Evans, G. R., Flowerdew, J., Hemri, S., Lerch, S., Roberts, N., Theis, S., Atencia, A., Ben Boualègue, Z., Bhend, J., Dabernig, M., De Cruz, L., Hieta, L., Mestre, O., Moret, L., Odak Plenkovič, I., Schmeits, M., Taillardat, M., Van den Bergh, J., Van Schaeybroeck, B., Whan, K. and Ylhaisi, J. (2021) Statistical postprocessing for weather forecasts – review, challenges and avenues in a big data world. *Bull. Amer. Meteorol. Soc.* **102**, E681–E699.
- Wagh, S., Kulkarni, R., Lonkar, P., Parde, A. N., Dhangar, N. G., Govardhan, G., Sajjan, V., Debnath, S., Gultepe, I., Rajeevan, M., Ghude, S. D. (2023) Development of visibility equation based on fog microphysical observations and its verification using the WRF model. *Model. Earth Syst. Environ.* **9**, 195–211.

- Wilks, D. S. (2018) Univariate ensemble postprocessing. In Vannitsem, S., Wilks, D. S., Messner, J. W. (eds.), *Statistical Postprocessing of Ensemble Forecasts*. Elsevier, Amsterdam, pp. 49–89.
- Wilks, D. S. (2019) *Statistical Methods in the Atmospheric Sciences*. 4th ed. Elsevier, Amsterdam.
- World Meteorological Organization (1992) *International Meteorological Vocabulary* (WMO-No.182). WMO, Geneva.
- World Meteorological Organization (2018) *Guide to Instruments and Methods of Observation. Volume I – Measurement of Meteorological Variables* (WMO-No.8). WMO, Geneva.
- Zhou, B., Du, J., Gultepe, I. and Dimego, G. (2012) Forecast of low visibility and fog from NCEP: Current status and efforts. *Pure Appl. Geophys.* **169**, 895–909.
- Zhou, B., Du, J., McQueen, J. and Dimego, G. (2009) Ensemble forecast of ceiling, visibility, and fog with NCEP Short-Range Ensemble Forecast system (SREF). *Aviation, Range, and Aerospace Meteorology Special Symposium on Weather–Air Traffic Management Integration*, Phoenix, AZ, American Meteorological Society, extended abstract 4.5. Available at: https://ams.confex.com/ams/89annual/techprogram/paper_142255.htm [Accessed on 25 October 2023]